

# Unraveling the Origin of Symmetry Breaking in H<sub>2</sub>O@C<sub>60</sub> Endofullerene Through Quantum Computations

Orlando Carrillo-Bohórquez,<sup>[a, b]</sup> Álvaro Valdés,<sup>[c]</sup> and Rita Prosimti<sup>\*[a]</sup>

We explore the origin of the anomalous splitting of the 1<sub>01</sub> levels reported experimentally for the H<sub>2</sub>O@C<sub>60</sub> endofullerene, in order to give some insight about the physical interpretations of the symmetry breaking observed. We performed fully-coupled quantum computations within the multiconfiguration time-dependent Hartree approach employing a rigorous procedure to handle such computationally challenging problems. We introduce two competing physical models, and discuss the observed unconventional quantum patterns in terms of anisotropy in the interfullerene interactions, caused by the change in the off-center position of the encapsulated water molecules inside the cage or the uniaxial C<sub>60</sub>-cage distortion, arising from noncovalent bonding upon water's encapsulation, or exohedral

fullerene perturbations. Our results show that both scenarios could reproduce the experimentally observed rotational degeneracy pattern, although quantitative agreement with the available experimental rotational levels splitting value has been achieved by the model that considers an uniaxial elongation of the C<sub>60</sub>-cage. Such finding supports that the observed symmetry breaking could be mainly caused by the distortion of the fullerene cage. However, as nuclear quantum treatments rely on the underlying interactions, a decisive conclusion hinges on the availability of their improved description, taken into account both endofullerene and exohedral environments, from forthcoming highly demanding electronic structure many-body interaction studies.

## Introduction

In recent years molecular endofullerenes, with several low-mass molecules (e.g. H<sub>2</sub>, HD, HF, H<sub>2</sub>O, CH<sub>4</sub>) encapsulated inside a fullerene cage, have been synthesized through clever routes/methods involving elaborated chemical and physical processes, like the multi-step organic synthesis procedure known as molecular surgery.<sup>[1–7]</sup> Such light-molecule endofullerenes have been then investigated using various spectroscopic techniques, e.g. infrared/far-infrared (IR/FIR), inelastic neutron scattering (INS), nuclear magnetic resonance (NMR), x-ray diffraction, and they found to exhibit unique and unconventional properties due to the highly quantum nature of the trapped molecule dynamics, specially evidence at the low-temperature experimental conditions.<sup>[3,8–16]</sup> In addition, some of these substances have also been of interest for potential long-term applications

to energy, gas storage and quantum information processing research.<sup>[1,9,17–24]</sup>


The endohedral water fullerene, H<sub>2</sub>O@C<sub>60</sub>, is one of particular interest, as water is a polar (triatomic) molecule, which also exhibits ortho/para nuclear spin isomerism, giving rise to additional quantum effects. Earlier INS, FTIR spectroscopy and cryogenic NMR experiments,<sup>[3]</sup> and more recent INS spectra<sup>[10]</sup> in highly pure samples of solid H<sub>2</sub>O@C<sub>60</sub> have revealed an energy splitting in the ground state of the encapsulated ortho-water, raising the 3-fold degeneracy into single and doublet states,<sup>[10]</sup> associated with symmetry-breaking of the water molecule environment.


Up to date, a variety of theoretical models and scenarios have been elaborated<sup>[16,25–29]</sup> to explore these experimental observations. In a series of studies, Bačić and co-workers<sup>[26,28,30,31]</sup> have performed 6D and 9D quantum calculations on translational-rotational and vibrational states of the H<sub>2</sub>O@C<sub>60</sub> system, while in order to treat the symmetry-lowering interactions, they have introduced electrostatic models involving dipole-dipole interactions between two neighbor H<sub>2</sub>O@C<sub>60</sub>, or quadrupole interactions between the charge densities of an encapsulated H<sub>2</sub>O molecule in a central C<sub>60</sub> cage surrounded by twelve empty ones. According to their quadrupole model, energy splittings of the ground ortho-H<sub>2</sub>O state have been observed in agreement with the experimental values only for the P orientation ordering of the C<sub>60</sub> cages. In the same vein, just recently the infrared absorption spectra of the endohedral water in solid mixture of C<sub>60</sub> have been recorded.<sup>[16]</sup> The fitting of these experimental data by a quantum mechanical model, including interactions of the H<sub>2</sub>O electric dipole and quadrupole moments with the electrostatic fields of the solid C<sub>60</sub>, has been reported,<sup>[16]</sup> and the cause of the H<sub>2</sub>O rotational levels splitting has been discussed in terms of effects of solid C<sub>60</sub> crystal field, change in H<sub>2</sub>O

[a] O. Carrillo-Bohórquez, R. Prosimti  
Institute of Fundamental Physics (IFF-CSIC), CSIC,  
Serrano 123, 28006 Madrid, Spain  
E-mail: rita@iff.csic.es

[b] O. Carrillo-Bohórquez  
Departamento de Física,  
Universidad Nacional de Colombia,  
Calle 26, Cra 39, Edificio 404, Bogotá, Colombia

[c] Á. Valdés  
Escuela de Física,  
Universidad Nacional de Colombia,  
Sede Medellín, A. A. 3840, Medellín, Colombia

 Supporting information for this article is available on the WWW under <https://doi.org/10.1002/cphc.202200034>

 © 2022 The Authors. ChemPhysChem published by Wiley-VCH GmbH. This is an open access article under the terms of the Creative Commons Attribution Non-Commercial License, which permits use, distribution and reproduction in any medium, provided the original work is properly cited and is not used for commercial purposes.

molecule geometry or translation-rotation couplings. Further, in an other recent work, symmetry arguments have been also employed<sup>[29,32]</sup> to construct a two-parameter  $S_6$  symmetry potential, in terms of translational and rotational states of a water molecule, and additional symmetry-lowering interactions, like the intramolecular Jahn-Teller cage distortion effects, have been investigated. Such adjusted model potential has been able to match the variations in energy from selected DFT calculations, and reproduce energy splittings similar to those of the quadrupole model.

As emphasized earlier,<sup>[27]</sup> in lack of full dimensional first-principles/*ab initio* interaction energies, we may speculate for various possible interaction terms in the potential and/or nuclear motion couplings, that could be able to match experimental evidences. In this vein, by introducing anisotropy in the  $n$ -mode potential expansion,<sup>[27]</sup> according to recent electronic structure calculations<sup>[33]</sup> and X-ray experimental evidences,<sup>[34]</sup> due to noncovalent interactions in interfullerene environment,<sup>[33,35–40]</sup> we have also computed rotational states splitting patterns in qualitative accord to those observed experimentally.<sup>[3,10]</sup>

Theoretical investigations of such unconventional features require fully coupled quantum treatments. Thus, recently we have reported such computational scheme, within the multi-configuration time-dependent Hartree (MCTDH) framework,<sup>[41,42]</sup> to perform in an efficient manner quantum dynamics calculations of any encapsulated triatomic molecule.<sup>[27,43,44]</sup> As mentioned, distinct suggestions have been reported for symmetry-lowering interaction,<sup>[3,9,16,25–29]</sup> including electrostatic charge-transfer, dipoles and quadrupoles between neighbor filled or empty cages, present of impurities, as well as crystal field effects, with the origin of such reduction in symmetry (from the  $I_h$  of the  $C_{60}$  molecule<sup>[45]</sup>) being of fundamental interest, whether it arises from inter-cage or intra-cage interactions or both.

Given the complexity of the problem, following by a quite complicated debate in the literature, and the lack of further decisive experimental observations, we introduce two competing physical models as a first attempt to identify the origin of the symmetry breaking. In order to address such issue quantitatively, we resort here to a computationally demanding approach to explore the effect of reduced endohedral/exohedral fullerene cage symmetry. Both models are alternative potential models, that are logically supported, and have been introduced by the need to understand complementary reasons (such as inter- and intra- fullerene interactions) about the origin of the symmetry breaking observed in the  $H_2O@C_{60}$ . Model (1) scenario considers anisotropy in the interfullerene interactions due to the change of water molecule configuration, *e.g.* such as an off-center position within the fullerene cage,<sup>[33,34]</sup> caused by the presence of significant electronic (noncovalent) intermolecular anisotropic interactions between it and the cage or neighbor ones. Model (2) incorporates anisotropy due to an uniaxial cage distortion. Such cage deformation could arise from the formation of O–H...C hydrogen bonds<sup>[33]</sup> under the encapsulation of the water molecule inside the  $C_{60}$  cage, and/or due to exohedral environment, like solid-state crystal effects or

anisotropic environment of the liquid crystal solvent.<sup>[3,9,46]</sup> Therefore, in the present study we have applied discrete gradual shifts of the encapsulated water molecule position from the  $C_{60}$ -cage center, or cage distortions (elongation and compression) along one direction of its original icosahedral symmetry structure, and then, the impact of such changes in water's configuration or  $C_{60}$ -cage modifications on the computed rotational energy splittings was evaluated.

## Computational Details and Models Under Consideration

In our previous work,<sup>[44]</sup> the exact kinetic energy operator has been derived for a nanoconfined light-heavy-light molecule, such as the water, and thus the Hamiltonian operator of the fully coupled  $H_2O@C_{60}$  reads:  $\hat{H} = -\frac{\hbar^2}{2M} \nabla_{\mathbf{R}}^2 - \frac{\hbar^2}{2m_H} \nabla_{\mathcal{R}_1}^2 - \frac{\hbar^2}{2m_H} \nabla_{\mathcal{R}_2}^2 + V(\mathbf{q})$ , with  $M = m_O + 2m_H$  being the total mass of the  $H_2O$ ,  $\mathbf{q}$  being the  $R, \beta, \alpha, \mathcal{R}_1, \mathcal{R}_2, \gamma, \phi, \theta, \chi$  coordinates, defined as  $R, \beta, \alpha$  ( $\mathcal{R}$ ) the spherical coordinates of the  $H_2O$  mass center with respect the space-fixed  $xyz$  coordinate system, the Radau  $\mathcal{R}_1, \mathcal{R}_2, \gamma$  coordinates describe the water molecule, and the  $\phi, \theta, \chi$  Euler angles. The potential operator is expressed as,  $V(\mathbf{q}) = V_{H_2O-C_{60}}(\mathbf{q}) + V_{H_2O}(\mathcal{R}_1, \mathcal{R}_2, \gamma)$ , where the  $V_{H_2O-C_{60}}$  potential is generated as a sum over the  $H_2O-C$  pairwise interactions, modeled with the H–C and O–C Lennard-Jones (LJ) 12–6 potentials adjusted to DFT-SAPT *ab initio* graphene-water reported in Ref. [47] while the water monomer potential, was taken from Ref. [48].

Within the MCTDH scheme<sup>[41,42]</sup> we used an  $n$ -mode representation of the potential,<sup>[49]</sup>  $V_M(Q_i) = V^{(0)} + \sum_{i=1}^7 V_i^{(1)}(Q_i) + \sum_{i=1, \neq j}^7 V_{ij}^{(2)}(Q_i, Q_j) + \dots + \sum_{i=1, \neq j, \neq k, \dots}^7 V_{ijk\dots}^{(7)}(Q_i, Q_j, Q_k, \dots)$ , with  $Q_1 = R$ ,  $Q_2 = [\beta, \alpha]$ ,  $Q_3 = \theta$ ,  $Q_4 = [\phi, \chi]$ ,  $Q_5 = \mathcal{R}_1$ ,  $Q_6 = \mathcal{R}_2$ , and  $Q_7 = \gamma$  a 7-mode combination scheme, and  $V^{(0)}$  being the reference configuration potential value,  $V^{(1)}$  the intramode terms, while the remaining  $V^{(n)}$  are the 2- up to 7-mode correlation terms. For affordable fully-coupled calculations we have considered  $n$ -mode selective representations of the  $V^{pD}$  potential, and the POTFIT algorithm,<sup>[50]</sup> as implemented in the MCTDH code,<sup>[41]</sup> was applied to transform each of them in a natural potential form.

In Figure 1 we show a schematic presentation of the water-cage interactions models employed. As mentioned, in order to understand complementary reasons about the origin of the symmetry breaking observed in the  $H_2O@C_{60}$ , we explore two alternative models that are logically supported. Thus, model (1) (see upper panel) represents a situation in which the  $C_{60}$  cage maintains its icosahedral symmetry, while the encapsulated water is shifted inside the cage and resided in an off-center position. Such scenario considers that the encaged water molecule is not chemically isolated, and thus the presence of significant electronic (noncovalent) intermolecular anisotropic interactions between it and the cage or neighbor ones. In this case, the  $V_{R_i}^{9D, vib} = V^{6D}(Q_1, Q_2, Q_3, Q_4) + \Delta V^{6D, vib}(Q_1^v; Q_3, Q_4, Q_5, Q_6, Q_7)$  potential, with  $\Delta V^{6D, vib}(Q_1^v; Q_3, Q_4, Q_5, Q_6, Q_7)$  given by  $V^{6D}(Q_3, Q_4, Q_5, Q_6, Q_7) - V^{3D}(Q_3, Q_4)$ , includes the combined coupling of the three vibrational  $\mathcal{R}_1, \mathcal{R}_2$  and  $\gamma$  degrees of freedom of the water molecule with the rotational  $\theta, \phi$  and  $\chi$  ones, where  $Q_1^v$  indicates the reference geometry in the  $n$ -mode expansion, and its value was chosen as the  $R_v$  variable to count for the interfullerene potential anisotropy.

In turn, model (2) describes modifications in the  $C_{60}$  cage structure, with its icosahedral symmetry broken by a perturbation in only one direction. Here we have applied the distortion along the  $x$ -axis, with  $y$  and  $z$  directions remaining equivalent, considering gradual uniaxial cage changes in both positive and negative  $x$ -axis directions, that result to elongation and contraction of the cage, respectively (see lower panel of Figure 1). Such model incorporates anisotropy due to external influences, such as the presence of occluded impurities and/or solid crystal effects, that may cause such deformations of the cage. Once we count the grade of the uniaxial cage deformation (in % elongation or contraction), the resulting potential  $V_{\%}^{9D^{def}}(Q_1, \dots, Q_7) = V^{6D^{def}}(Q_1, Q_2, Q_3, Q_4) + \Delta V^{6D_{R1}^{def}}(Q_2, Q_3, Q_4, Q_5) + \Delta V^{6D_{R2}^{def}}(Q_2, Q_3, Q_4, Q_6) + \Delta V^{6D_{R3}^{def}}(Q_2, Q_3, Q_4, Q_7)$ , takes into account the internal coordinates of the water molecule, as well as the position of its center of mass with respect to the distorted- $C_{60}$  cage, with  $V^{6D^{def}}(Q_1, Q_2, Q_3, Q_4)$  term being the exact potential representation of the 6D (rotational and translational degrees of freedom) system, and  $\Delta V^{6D_{i}}(Q_i, Q_2, Q_3, Q_4)$  with  $i=1, 5, 6, 7$  the corresponding terms in the expansion, keeping fixed at their equilibrium values the independent degrees of freedom at each potential term.

For each water-cage model, the Hamiltonian operator used in the 9D MCTDH calculations is expressed in a primitive discrete-variable-representation (DVR) basis sets grid of 25 harmonic oscillator (HO) in the range of (0.65, 1.27) Å and 25 radial form solutions (rHO) in the range of (0, 0.38) Å, in  $\mathcal{R}_1, \mathcal{R}_2$ , and  $R$  coordinates, respectively, 35 Legendre (Leg) in the range of (0,  $\pi$ ) and 25 restricted Legendre-type (Leg/R) DVR functions in the range of (1.26, 2.65) rad in each of  $\beta, \theta$ , and  $\gamma$  angles, respectively, and 35 exponential (exp) DVR functions in each  $\alpha, \chi$  and  $\phi$ , coordinates in the range of (0,  $2\pi$ ). We performed block-improved-relaxation (BIR) MCTDH calculations,<sup>[41,51]</sup> and a number of 4, 12, 25, 60, 3, 3, and 3 single-particle functions (SPFs) in each of  $Q_i$  with  $i=1-7$  combination mode was needed to obtain well-converged energy values for the ground and 42 lower rotationally excited states of the  $H_2O@C_{60}$  in each model case.

## Results and Discussion

In Figure 2 we display potential energy curves as a function of the Cartesian  $x, y$  and  $z$  coordinates for three different values of

the  $R_v$  anisotropic parameter, according to the model (1). The potential curves are obtained by minimizing the water- $C_{60}$  interaction along each  $x/y/z$  position of its mass center.

As expected, for  $R_v=0$  we obtained a symmetric double-minima topology along all  $x/y/z$  coordinates, and as the  $R_v$  value increases, the topology is maintained in the  $x$  direction, while for both  $y$  and  $z$  coordinates we observed the appearance of an asymmetric double-well. Such possible source of anisotropy, considered in model (1), could correspond to the presence of weak noncovalent electronic interactions between the water and the  $C_{60}$  cage, causing changes only in the water's molecule configuration inside the cage, and thus symmetry breaking with fingerprints in the pattern of rotational quantum states.

With this in mind, in Table S1 (see in supporting information material) we list the calculated relative energy values of the  $1_{01}, 1_{11}$  and  $1_{10}$  rotational levels obtained from the 9D BIR/MCTDH computations, and in Figure 2 we depict (see in lower panel) their evolution as a function of the  $R_v$  interfullerene potential anisotropy parameter of model (1). One can see that significant energy splittings are observed for all rotational levels presented in the figure for  $R_v \geq 0.2$  bohr, and their values are increased as  $R_v$  increases. In particular, we found that the ground ortho- $H_2O$  triplet  $1_{01}$  state shows a splitting into the  $1_{01}^{a,d}$  doublet and singlet  $1_{01}^b$  states, keeping the same 2:1 splitting pattern for all  $R_v$  up to 0.8 bohr studied here. The same behavior is observed also for the first rotationally excited  $1_{11}$  para- $H_2O$  state, although with somehow smaller splitting values, while the  $1_{10}$  ortho- $H_2O$  state exhibits an opposite 1:2 energy splitting pattern than the ground  $1_{01}$  ortho- $H_2O$  state.

Such degeneracy lifting has been one of the most interesting aspect observed experimentally for the ground  $1_{01}$  ortho- $H_2O$  state of the  $H_2O@C_{60}$  systems, and splitting values of  $4.8 \pm 0.8$  and  $4.2 \pm 0.2$   $cm^{-1}$  have been reported from the INS and FIR spectra studies,<sup>[3,10]</sup> with a splitting pattern being originally of 2:1,<sup>[10]</sup> and 1:2 from a later analysis (see discussion in Ref. [26]). So, if one follows the evolution of the energy splitting of the  $1_{01}$  levels *versus*  $R_v$  (see lower panel of Figure 2)

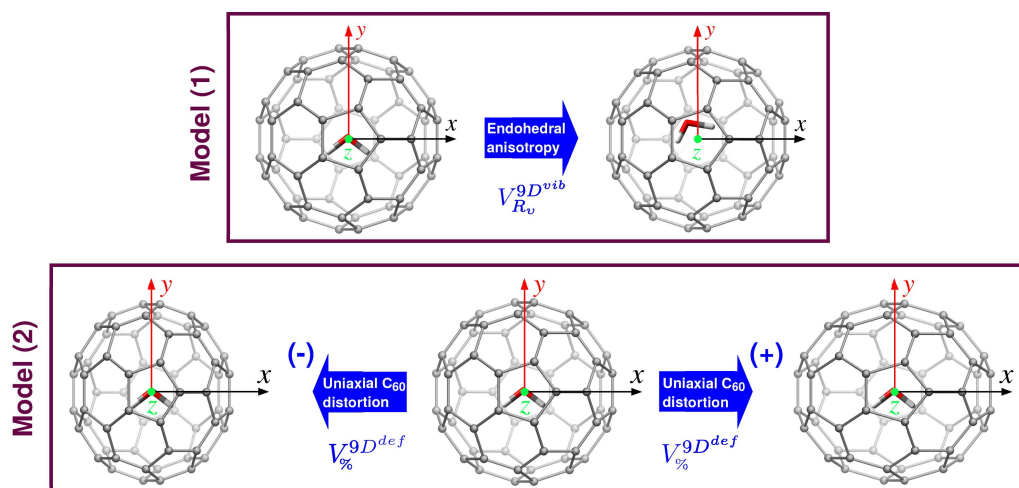


**Figure 1.** Schematic representation of the water-cage models introduced in this study. The space-fixed coordinate system is also displayed, with its origin at the center of the  $C_{60}$  cage.

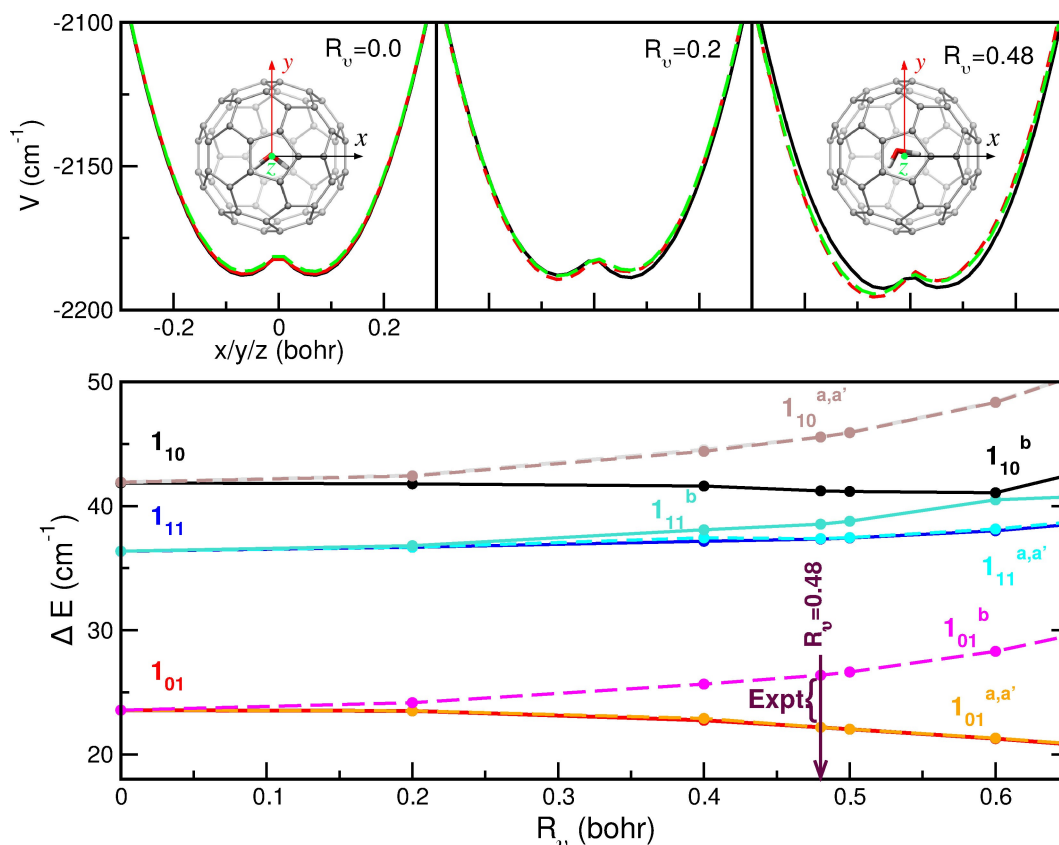


**Figure 2.** Minimum energy potential curves obtained (upper panels) from the model (1) for the indicated values of  $R_v$  anisotropy parameter (see  $V_{R_v}^{2D^{orb}}$  potential). Color black/red/green lines indicate each  $x/y/z$  axis, respectively (see inset plot). Evolution of the indicated rotational state energies as a function of the  $R_v$  (lower panel). The ortho- $H_2O$  triplet  $1_{01}$  state splits into the  $1_{01}^{a,a'}$  doublet (orange/red color lines) and singlet  $1_{01}^b$  (magenta color line), the  $1_{11}$  into  $1_{11}^{a,a'}$  (blue/cyan color lines) and  $1_{11}^b$  (turquoise color line), while the  $1_{10}$  into  $1_{10}^b$  (black color lines) and  $1_{10}^{a,a'}$  (brown/grey color lines) as the  $R_v$  parameter increases. Rotational energies are referred with respect to the ground state  $0_{00}$  energy obtained from the MCTDH computations.

can see that for  $R_v = 0.48$  bohr the theoretical estimated value of  $4.2 \text{ cm}^{-1}$  matches the most recent experimentally measured one, although the predicted pattern for ground ortho- $H_2O$  state is found to be 2:1, in reverse order than the latter experimental data analysis.

In turn, we proceed with results from model (2), and in the upper panels of Figure 3 we display potential energy (relative values with respect to minimum energy) curves as a function of the Cartesian  $x$ ,  $y$  and  $z$  coordinates for distortion values of  $-0.93$  and  $+1.1\%$ , corresponding to an uniaxial contraction and elongation along the  $x$ -axis of the  $C_{60}$  cage, respectively, comparing them with the unperturbed (0%)  $C_{60}$  cage. Significant changes in the potential curves along  $x$ -axis are present, which can be clearly observed in the figure at energies above the ground  $0_{00}$  state, in both uniaxial  $C_{60}$  distortion cases. In the lower panel of Figure 3, we plot the calculated relative energy values of the three lower  $1_{01}$ ,  $1_{11}$  and  $1_{10}$  rotational levels of the  $H_2O@C_{60}$  from the the 9D BIR/MCTDH computations as a function of the distortion (%) parameter of the model (2), while in Table S2 (see in supporting information material) all computed values for distortion values of  $-2.5$  to  $+2.5\%$  are given.

As it can be seen, when the  $C_{60}$  cage is deformed, all 3-fold  $J=1$  degenerated rotational levels are splitted into doublets and singlets (2:1) or *vice-versa* (1:2) depending on the direction of the  $C_{60}$  cage distortion along  $x$ -axis, such as compression or elongation, respectively. Again, we have reproduced the reported experimental splitting energy value of the  $1_{01}$  ortho- $H_2O$  state of the  $H_2O@C_{60}$  system, with a compression and an elongation of the  $C_{60}$  cage along  $x$  axis of  $-0.93$  and  $+1.1\%$ , respectively, of its initial length (see Figure 3). For the  $1_{01}$  level the computed splitting pattern is 2:1 for the contraction of the cage, and 1:2 for the elongation, all over the  $x$ -axis of distortion. The same behavior is also observed for the  $1_{11}$  levels, although their energy splittings are found to be much smaller, of less than  $1 \text{ cm}^{-1}$ , than those of the  $1_{01}$ , while the  $1_{10}$  shows the opposite splitting pattern under contraction/elongation of the  $C_{60}$  cage compared to the  $1_{01}$  state, with similar energy values of around  $4.5 \text{ cm}^{-1}$  at distortions of  $-0.93$  and  $+1.1\%$ .

Furthermore, one should notice (see Figures 2 and 3) the similarities between the evolution of the  $1_{01}$ ,  $1_{11}$  and  $1_{10}$  rotational states as a function of the  $R_v$  and contraction parameters, as well as the corresponding energy splitting patterns. Both model (1) and model (2) (contraction case) found to provide similar results, while model (2) (elongation case)

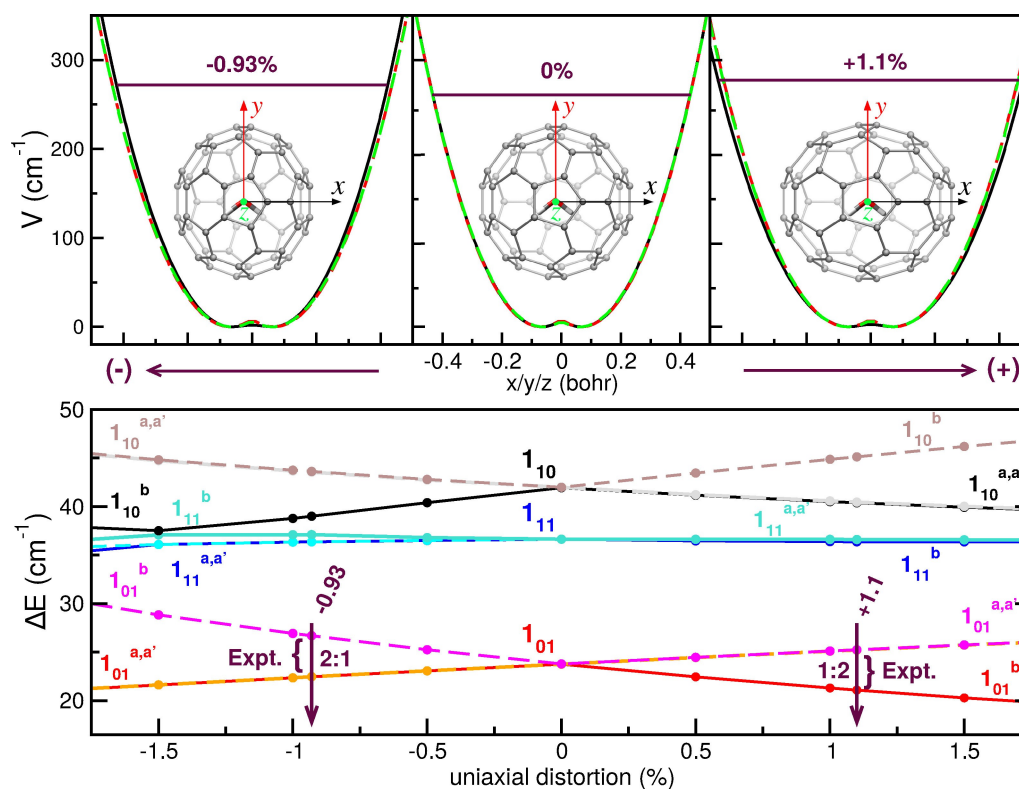


**Figure 3.** Minimum energy potential curves obtained (upper panels) for the indicated values of the  $C_{60}$ -cage distortion (%) from the model (2) (see  $V_{\%}^{2D^{def}}$  potential). As in Figure 2, the black solid and red/green color dashed lines indicated the  $x$  and  $y/z$  axes, respectively (see inset plot therein), while horizontal dark solid line indicates the zero point energy ( $0_{00}$  state) in each case. Evolution of the indicated rotational state energies as a function of the uniaxial distortion (%) of the  $C_{60}$  cage (lower panel). As in Figure 2, the  $1_{01}$ ,  $1_{11}$ , and  $1_{10}$  triplet splits into doublet  $1_{01}^{a,a'}$  and singlet  $1_{01}^b$  states as the uniaxial distortion of the the  $C_{60}$  cage increases or decreases (see color lines). Rotational energies are referred with respect to the ground state  $0_{00}$  energy.

seems to be the closer match with the most recent experimental evidences on the  $1_{01}$  1:2 splitting pattern.<sup>[10,26]</sup>

The fact that both model (1) and (2) were able to reproduce the splitting of the  $1_{01}$  energy level introducing a single potential parameter counting the endohedral anisotropy or uniaxial cage distortion suggests that such interactions could be the main sources of the observed symmetry-lowering. Therefore, in Figure 4 we show the results obtained of our models, considering the “best-performed” parameter values (see also Table S3 in supporting information material), for states higher in energy, with  $J$  up to 2, and their comparison with all extant experimental data<sup>[3,10]</sup> from the INS spectra including their corresponding experimental uncertainties. The energies of the icosahedral symmetry model are also depicted in the figure for comparison reasons.

One can see that, as in the  $J=1$  states, energy splittings of similar values are also computed for the  $J=2$   $H_2O@C_{60}$  levels with various splitting patterns, e.g. 1.0 and 4.4  $cm^{-1}$  with 1:2:2 for the  $2_{02}$  or 2.0  $cm^{-1}$  for the  $2_{21}$  (see in more detail in Table S3 in supporting information material for model(2)). However, the reported experimental INS results have errors of  $\pm 0.4$   $cm^{-1}$  for the  $1_{01}^{a,a'}$  and  $2_{12}$ ,  $\pm 0.8$   $cm^{-1}$  for the  $2_{21}$ , or  $\pm 1.2$   $cm^{-1}$  for the  $1_{11}$ ,  $2_{02}$  and  $2_{20}$  up to  $\pm 5$   $cm^{-1}$ <sup>[3,10]</sup> for the  $1_{10}$  (see Figure 4), so within the experimental uncertainties there are certainly several

unresolved splittings, and further experimental data are needed to resolve such issue.

Thus, in lack of extra experimental data in Figure 5 we also present comparisons with rotational energy values from previous theoretical models available in the literature.<sup>[16,26,28,29]</sup> In particular, we have considered the electrostatic quadrupolar model,<sup>[26,28]</sup> the more recent  $S_6$  symmetry-adapted potential model,<sup>[29]</sup> as well as the IR spectral fitting model.<sup>[16]</sup> Both earlier models<sup>[26,28,29]</sup> contain “ad-hoc” assumptions and parameters, such as considering one central  $H_2O$ -occupied  $C_{60}$  cage surrounding by twelve empty near-neighbor cages, all of them rigid with icosahedral symmetry and in P orientational orderings, with a variable water dipole moment value, or unknown free parameters chosen to reproduce results of the electrostatic model up to 12 meV, while the parameters of the spectral model<sup>[16]</sup> have been determined by fits to the synthetic experimental IR absorption spectra of solid  $H_2O@C_{60}$  samples at liquid helium temperature.<sup>[16]</sup> In the present models (1) and (2) the proposition is that the symmetry breaking arises predominantly from intermolecular anisotropy due to interfullerene interactions or exohedral perturbations, and the corresponding adjustable parameter,  $R_v$  or cage distortion (%), has been determined by matching only the energy splitting of the  $1_{01}^{a,a'}$  and  $1_{01}^b$  levels to the experimental value. In addition, we found that model (2) also matches the splitting pattern of 1:2 in

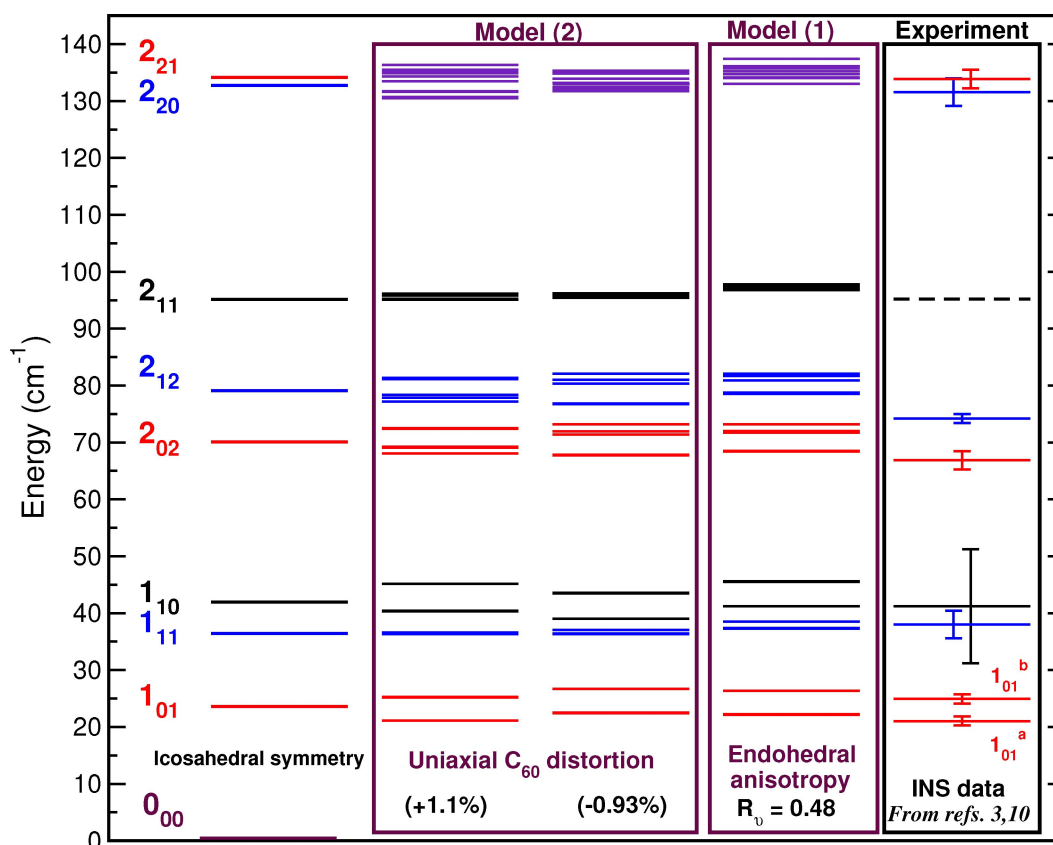


**Figure 4.** Computed rotational energy levels using model (1) and (2) developed in this work, and their comparison with the experimental data available from INS spectra.<sup>[3,10]</sup> Purple color lines correspond to unresolved parity symmetry energy levels (see Table S3). Experimental uncertainties are shown with error bars, while dashed line represents levels of the gas water, as they are not resolved in the INS data.

accord with the latter experimental INS spectra analysis<sup>[10,26]</sup> and electrostatic interaction model.<sup>[26,28]</sup> Further, we should mention here some evidence for a distortion in the electronic distribution of the cage (and possibly geometric distortion) through solid-state NMR measurements<sup>[8]</sup> could also support model (2) estimates.

Definitely, the ability of a proposed model to reproduce very well the available experimental measurements suggests certain arguments in favor of its main assumptions. In Figure 5 one can see that the results of the present model (2) are found in a quite good accord with the energies obtained from the electrostatic quadrupolar model,<sup>[26,28]</sup> while notable quantitative differences were found with the data from the  $S_6$  symmetry-adapted potential<sup>[29]</sup> and the IR spectral fit models.<sup>[16]</sup> The observed deviations are considerable for the higher  $2_{21}$  and  $2_{20}$  rotational energy levels in both cases, as well as for the  $1_{11}$  and  $1_{10}$  energies from the spectral fit models.<sup>[16]</sup> Our study demonstrates that endofullerene anisotropy or exohedral distortion could give close matches to the INS spectra value available, and thus should be considered. However, such discrepancies between the results obtained from various available models, based on different hypothesis or assumptions, could indicate possible complementary contribution/s from additional mechanisms or interactions for the symmetry breaking observed in  $H_2O@C_{60}$  and similar endofullerenes. Thus, once again we

should emphasize the importance of an accurate and reliable description of the many-body interactions between the encapsulated molecule and its surrounding environment (inter/intra-cage and solid crystal effects).

## Summary and Conclusions

We have introduced two different competing physical models to investigate the predominant source of symmetry breaking observed experimentally in the  $H_2O@C_{60}$  endofullerene. Such lowering of symmetry induced splitting of the three-fold degenerate ground state of the ortho- $H_2O$  endofullerene into a double and single energy states of about  $4\text{ cm}^{-1}$ . Both models incorporate anisotropy in the potential form: model (1), through the  $R_v$  parameter, introduces off-cage-center effects due to electronic (noncovalent) intermolecular interactions between water molecule and the cage, while model (2) describes modifications in the  $C_{60}$  cage structure applying distortion along its x-axis due to possible external influences. For each model, we have performed rigorous quantum calculations within the MCTDH framework, to handle efficiently the full 9D problem. The  $C_{60}$  cage is considered rigid, while all intermolecular and intramolecular degrees of freedom of the encapsulated water molecule are fully coupled. The calculations yield well-con-

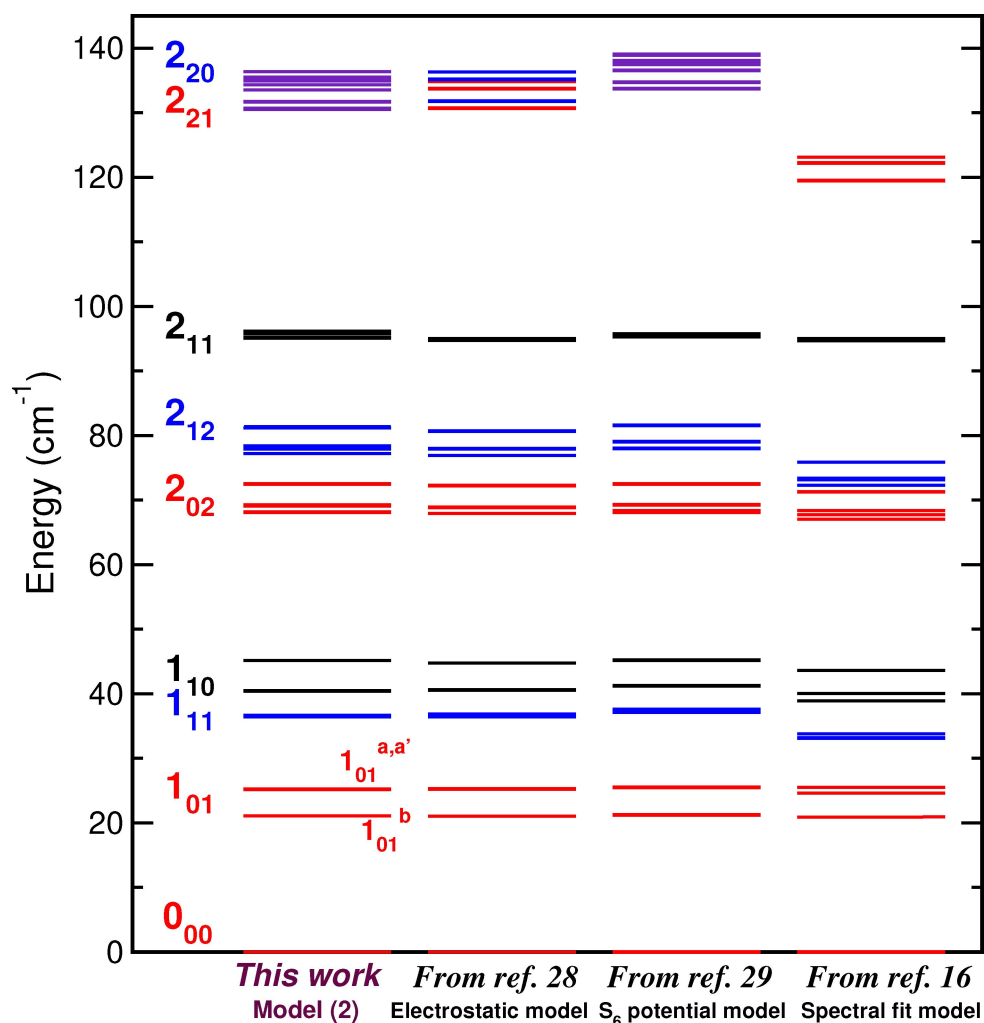


**Figure 5.** Rotational energy levels obtained from the present 9D MCTDH calculations, compared with those values from models reported previously in Refs. [16,28] and [29].

verged energies of various low-lying rotational levels. Their values and those of the corresponding level splittings are compared with previously reported data from both theoretical studies and experimental measurements.

Among many other possible sources, we found that a small deformation of the  $C_{60}$  cage, or inducing a slight change in the off-center position of the encapsulated water molecule inside the cage, can reproduce the rotational levels splitting, observed experimentally. Although we should note that model (1) predicts a reverse order pattern for such splitting. Such failure to reproduce quantitative details, indicates that model (1) needs further refinement in order to describe correctly the anisotropy in the underlying interactions, and thus should be treated as a first attempt to represent the presence of rather substantial water-cage interactions in the  $H_2O@C_{60}$  reported in recent electronic structure studies and X-ray experiments. Our focus has been on developing models that could allow to generate insights into the effect of inter- intra-fullerene interactions on the rotational splitting, recognizing that there are limitations for providing an overall agreement, and highlighting continuously

the importance of an accurate/reliable representation of the PES, as well as decisive experimental measurements for higher lying states.

The results obtained are quite surprising, as both models considered here are conceptually based on distinct ideas for the source of the symmetry-breaking, such as due to anisotropy in the endofullerene environment (presence of significant non-covalent guest-host interactions) or distortion by exohedral interactions (presence of impurities and lattice effects). The INS data clearly evidence such symmetry-breaking for the ground ortho-water with a significant splitting of this level of the encapsulated water molecule. Such data from experimental observations are available only for the ground  $1_{01}^{a,a'}$  ortho- $H_2O$  state, while the theoretical studies predict the lifting of degeneracy for higher excited rotationally states, too. Just recently, an energy splitting of  $2.9\text{ cm}^{-1}$  has been also reported<sup>[16]</sup> for the translational transition  $N=0 \rightarrow N=1$  of ortho- $H_2O$  from IR absorption spectroscopy experiments, while X-ray experiments coupled with DFT and molecular dynamics simulations have just shown that  $H_2O$  is located at an off-center

position inside the  $C_{60}$ .<sup>[34]</sup> Definitely, the observation of such phenomena requires deeper investigation from both theory and experiment. As the nature of the observed symmetry breaking can have a very subtle origin, apart of decisive experimental measurements of higher lying states for the  $H_2O@C_{60}$  endofullerene, theoretical treatments especially on the electronic structure many-body interactions are highly demanded in order to provide conclusive insights on the symmetry-lowering effects.

Obviously, the lack of such accurate potentials is what restrict to approximate models in describing the interactions. Fully coupled exact quantum methodologies rely on realistic underlying forces obtained from first-principles approaches. Although, the ability of the proposed models to reproduce experimental measurements in quantitative accord accounts in favor of its main assumptions, definitive results highly depend on improved full-dimensional descriptions of the corresponding intermolecular PESs. The sum of pairwise potentials approach employed to construct the 9D potential surface is unable to represent higher n-body effects in the weak noncovalent electronic interactions between the encapsulated water molecule and the surrounding  $C_{60}$  cage environment. Although, the present results are obtained from numerically exact quantum computations, they are constrained by the lack of such many-body contributions in the confining potential, that could introduce anisotropy in a proper manner, affecting the quality and reliability of the employed PES. A full understanding can be only achieved by developing, testing and validating models, that involves various levels of quantum theory and their application to similar nanoconfined systems, such as  $HF@C_{60}$ , etc. Thus, from the theoretical point of view, this leaves room for further research, that should be first focused on a realistic, first-principles representation of the interfullerene interactions, following by additional investigations of the intrafullerene and periodic crystal packing effects.

## Acknowledgement

The authors thank to Centro de Calculo del IFF, SGAI (CSIC) and CESGA for allocation of computer time. We acknowledge financial support by MINECO grant No. FIS2017-83157-P, MICINN grant No, PID2020-114654GB-I00, COST Action CA18212(MD-GAS), and the Universidad Nacional de Colombia Hermes code: 49572. O.C.B. acknowledges the SEGIB Research Fellowship (C.2020) – The Carolina Foundation.

## Conflict of Interest

The authors declare no conflict of interest.

## Data Availability Statement

The data that support the findings of this study are available in the supplementary material of this article.

**Keywords:** computational quantum treatments · light-molecule endofullerenes · model potentials · nanoconfined molecules · rotational splitting

- [1] K. Komatsu, M. Murata, Y. Murata, *Science* **2005**, *307*, 238–240.
- [2] K. Kurotobi, Y. Murata, *Science* **2011**, *333*, 613–616.
- [3] C. Beduz, M. Carravetta, J. Y.-C. Chen, M. Concistré, M. Denning, M. Frunzi, A. J. Horsewill, O. G. Johannessen, R. Lawler, X. Lei, M. H. Levitt, Y. Li, S. Mamone, Y. Murata, U. Nagel, T. Nishida, J. Ollivier, S. Rols, T. Roöm, R. Sarkar, N. J. Turro, Y. Yang, *Proc. Nat. Acad. Sci.* **2012**, *109*, 12894–12898.
- [4] J. Y.-C. Chen, Y. Li, M. Frunzi, X. Lei, Y. Murata, R. G. Lawler, N. J. Turro, *Philos. Trans. R. Soc. A* **2013**, *371*, 20110628.
- [5] R. Zhang, M. Murata, T. Aharen, A. Wakamiya, T. Shimoaka, T. Hasegawa, Y. Murata, *Nat. Chem.* **2016**, *8*, 435–441.
- [6] Y. Morinaka, R. Zhang, S. Sato, H. Nikawa, T. Kato, K. Furukawa, M. Yamada, Y. Maeda, M. Murata, A. Wakamiya, S. Nagase, T. Akasaka, Y. Murata, *Angew. Chem. Int. Ed.* **2017**, *56*, 6488–6491; *Angew. Chem.* **2017**, *129*, 6588–6591.
- [7] S. Bloodworth, G. Sotinova, S. Alom, S. Vidal, G. R. Bacanu, S. J. Elliott, M. E. Light, J. M. Herniman, G. J. Langley, M. H. Levitt, et al., *Angew. Chem. Int. Ed.* **2019**, *58*, 5038–5043; *Angew. Chem.* **2019**, *131*, 5092–5097.
- [8] M. Concistré, S. Mamone, M. Denning, G. Pileio, X. Lei, Y. Li, M. Carravetta, N. Turro, M. Levitt, *Philos. Trans. R. Soc. A* **2013**, *371*, 20120102.
- [9] M. H. Levitt, *Phil. Trans. R. Soc. A* **2013**, *371*, 20120429.
- [10] K. S. K. Goh, M. Jimenez-Ruiz, M. R. Johnson, S. Rols, J. Ollivier, M. S. Denning, S. Mamone, M. H. Levitt, X. Lei, Y. Li, N. J. Turro, Y. Murata, A. J. Horsewill, *Phys. Chem. Chem. Phys.* **2014**, *16*, 21330–21339.
- [11] S. Mamone, M. Concistré, E. Carignani, B. Meier, A. Krachmalnicoff, O. G. Johannessen, X. Lei, Y. Li, M. Denning, M. Carravetta, K. Goh, A. J. Horsewill, R. J. Whitby, M. H. Levitt, *J. Chem. Phys.* **2014**, *140*, 194306.
- [12] S. J. Elliott, C. Bengs, K. Kouril, B. Meier, S. Alom, R. J. Whitby, M. H. Levitt, *ChemPhysChem* **2018**, *19*, 251–255.
- [13] K. Kouřil, B. Meier, S. Alom, R. J. Whitby, M. H. Levitt, *Faraday Discuss.* **2018**, *212*, 517–532.
- [14] B. Meier, K. Kouřil, C. Bengs, H. Kouřilová, T. C. Barker, S. J. Elliott, S. Alom, R. J. Whitby, M. H. Levitt, *Phys. Rev. Lett.* **201**, *120*, 266001.
- [15] H. Suzuki, M. Nakano, Y. Hashikawa, Y. Murata, *J. Phys. Chem. Lett.* **2019**, *10*, 1306–1311.
- [16] A. Shugai, U. Nagel, Y. Murata, Y. Li, S. Mamone, A. Krachmalnicoff, S. Alom, R. J. Whitby, M. H. Levitt, T. Roöm, *J. Chem. Phys.* **2021**, *154*, 124311.
- [17] S. Yang, C.-R. Wang, *Endohedral fullerenes: From fundamentals to application*, World Scientific, 2014.
- [18] R. B. Ross, C. M. Cardona, D. M. Guldi, S. G. Sankaranarayanan, M. O. Reese, N. Kipidakis, J. Peet, B. Walker, G. C. Bazan, E. Van Keuren, B. C. Holloway, M. Drees, *Nat. Mater.* **2011**, *8*, 208–212.
- [19] O. Echt, T. Mark, P. Scheier, *Handbook of Nanophysics, Vol. 2: Clusters and Fullerenes*, CRC Press, Taylor and Francis Group, Boca Raton, **2010**.
- [20] M. Frunzi, S. Jockusch, J. Y.-C. Chen, R. M. K. Calderon, X. Lei, Y. Murata, K. Komatsu, D. M. Guldi, R. G. Lawler, N. J. Turro, *J. Am. Chem. Soc.* **2011**, *133*, 14232–14235.
- [21] M. Baskar, N. Sathyan, T. G. Nair, et al., *J. Biophys. Chem.* **2018**, *9*, 15.
- [22] J. Twamley, *Phys. Rev. A* **2003**, *67*, 052318.
- [23] W. Harneit, *Phys. Rev. A* **2002**, *65*, 032322.
- [24] R. Zhang, M. Murata, A. Wakamiya, T. Shimoaka, T. Hasegawa, Y. Murata, *Sci. Adv.* **2017**, *3*, e1602833.
- [25] P. M. Felker, Z. Bačić, *J. Chem. Phys.* **2017**, *146*, 084303.
- [26] P. M. Felker, V. Vlček, I. Hietanen, S. FitzGerald, D. Neuhauser, Z. Bačić, *Phys. Chem. Chem. Phys.* **2017**, *19*, 31274–31283.
- [27] A. Valdés, O. Carrillo-Bohórquez, R. Prosmi, *J. Chem. Theory Comput.* **2018**, *14*, 6521–6531.
- [28] Z. Bačić, V. Vlček, D. Neuhauser, P. M. Felker, *Faraday Discuss.* **2018**, *212*, 547–567.
- [29] E. Rashed, J. L. Dunn, *Phys. Chem. Chem. Phys.* **2019**, *21*, 3347–3359.
- [30] P. M. Felker, Z. Bačić, *J. Chem. Phys.* **2016**, *144*, 201101.
- [31] P. M. Felker, Z. Bačić, *J. Chem. Phys.* **2020**, *152*, 014108.
- [32] J. L. Dunn, E. Rashed, *J. Phys. Conf. Ser.* **2018**, 012003.
- [33] A. Varadwaj, P. R. Varadwaj, *Chem. Eur. J.* **2012**, *18*, 15345–15360.
- [34] S. P. Jarvis, H. Sang, F. Junqueira, O. Gordon, J. E. A. Hodgkinson, A. Saywell, P. Rahe, S. Mamone, S. Taylor, A. Sweetman, J. Leaf, D. A.



- Duncan, T.-L. Lee, P. K. Thakur, G. Hoffman, R. J. Whitby, M. H. Levitt, G. Held, L. Kantorovich, P. Moriarty, R. G. Jones, *Commun. Chem.* **2021**, *4*, 135.
- [35] K. Yagi, D. Watanabe, *Int. J. Quantum Chem.* **2009**, *109*, 2080–2090.
- [36] T. Korona, H. Dodziuk, *J. Chem. Theory Comput.* **2011**, *7*, 1476–1483.
- [37] S. Aoyagi, N. Hoshino, T. Akutagawa, Y. Sado, R. Kitaura, H. Shinohara, K. Sugimoto, R. Zhang, Y. Murata, *Chem. Commun.* **2014**, *50*, 524–526.
- [38] O. V. de Oliveira, A. da Silva Goncalves, *Comput. Chem.* **2014**, *2*, 51–58.
- [39] A. Galano, A. Pérez-González, L. del Olmo, M. Francisco-Marquez, J. R. León-Carmona, *J. Mol. Model.* **2014**, *20*, 2412.
- [40] A. Jaroš, Z. Badri, P. L. Bora, E. F. Bonab, R. Marek, M. Straka, C. Foroutan-Nejad, *Chem. Eur. J.* **2018**, *24*, 4245–4249.
- [41] G. A. Worth, M. H. Beck, A. Jäckle, H.-D. Meyer, The MCTDH Package, Version 8.2, (2000). H.-D. Meyer, Version 8.3 (2002), Version 8.4 (2007). See <http://mctdh.uni-hd.de>.
- [42] H.-D. Meyer, *WIREs Comput. Mol. Sci.* **2012**, *2*, 351–374.
- [43] A. Valdes, D. J. Arismendi-Arrieta, R. Prosimiti, *J. Phys. Chem. C* **2015**, *119*, 3945–3956.
- [44] O. Carrillo-Bohorquez, A. Valdes, R. Prosimiti, *J. Chem. Theory Comput.* **2021**, *17*, 5839–5848.
- [45] E. F. Sheka, B. S. Razbirin, D. K. Nelson, *J. Phys. Chem. A* **2011**, *115*, 3480–3490.
- [46] G. B. Alers, B. Golding, A. R. Kortan, R. C. Haddon, F. A. Theil, *Science* **1992**, *257*, 511–514.
- [47] A. B. Farimani, Y. Wu, N. R. Aluru, *Phys. Chem. Chem. Phys.* **2013**, *15*, 17993–18000.
- [48] O. L. Polyansky, P. Jensen, J. Tennyson, *J. Chem. Phys.* **1996**, *105*, 6490–6497.
- [49] S. Carter, S. J. Culik, J. M. Bowman, *J. Chem. Phys.* **1997**, *107*, 10458–10469.
- [50] A. Jäckle, H.-D. Meyer, *J. Chem. Phys.* **1998**, *109*, 3772–3779.
- [51] L. J. Doriol, F. Gatti, C. Iung, H.-D. Meyer, *J. Chem. Phys.* **2008**, *129*, 224109.

---

Manuscript received: January 17, 2022  
Revised manuscript received: February 1, 2022  
Version of record online: March 14, 2022